J|A|C|S ARTICLES

Published on Web 11/05/2010

Degradation Patterns in Water and Oxygen of an Inverted Polymer Solar Cell

Kion Norrman, Morten V. Madsen, Suren A. Gevorgyan, and Frederik C. Krebs*

Risø National Laboratory for Sustainable Energy, Technical University of Denmark, Frederiksborgvej 399, DK-4000 Roskilde, Denmark

Received July 16, 2010; E-mail: frkr@risoe.dtu.dk

Abstract: The spatial distribution of reaction products in multilayer polymer solar cells induced by water and oxygen atmospheres was mapped and used to elucidate the degradation patterns and failure mechanisms in an inverted polymer solar cell. The active material comprised a bulk heterojunction formed by poly(3-hexylthiophene) (P3HT) and [6,6]-phenyl-C61-butyric acid methyl ester (PCBM) sandwiched between a layer of zinc oxide and a layer of poly(3,4-ethylenedioxythiophene) poly(styrenesulfonate) (PEDOT:PSS) that acted as, respectively, electron and hole transporting layers between the active material and the two electrodes indium−tin−oxide (ITO) and printed silver. X-ray photoelectron spectroscopy (XPS) and time-of-flight secondary ion mass spectrometry (TOF-SIMS) in conjunction with isotopic labeling using $H_2{}^{18}O$ and $^{18}O_2$ enabled detailed information on where and to what extent uptake took place. A comparison was made between the use of a humid (oxygen-free) atmosphere and a dry oxygen atmosphere during testing of devices that were kept in the dark and devices that were subjected to illumination under simulated sunlight. It was found that the reactions taking place at the interface between the active layer and the PEDOT:PSS were the major cause of device failure in the case of these inverted devices, which are compatible with full roll-to-roll (R2R) coating and industrial manufacture. The PEDOT:PSS was found to phase separate, with the PEDOT-rich phase being responsible for most of the interface degradation in oxygen atmospheres. In water atmospheres, little chemically induced degradation was observed, whereas a large partially reversible dependence of the open circuit voltage on the relative humidity was observed. In addition, temporal aspects are discussed in regard to degradation mechanisms. Finally, analytical aspects in regard to storing devices are discussed.

Introduction

Polymer solar cells convey several advantages such as flexibility, they are lightweight, environmental friendliness, a low thermal budget, low cost, and very fast modes of production by printing techniques.[1−10] From a production point of view, it is desirable to manufacture polymer solar cells entirely using printing techniques, that is, from solution without any vacuum steps involved.[11,12] The limiting factor is the lack of an acceptable substitute for indium−tin−oxide (ITO) as a transparent electrode, which is typically deposited by sputtering (i.e., in a vacuum). The current performance of the technology is limited (as compared to silicon-based solar cells) by mainly two factors: (i) the efficiency, which is on the order of 5% (although a few reports of efficiencies approaching higher values in the 6−8% range have appeared recently),[13,14] and (ii) the lifetime, which is on the order of years under outdoor conditions[15,16] with good stability being recorded for both air stable devices and encapsulated devices.[17,18] As a consequence, efficiency and stability have become important research areas within polymer solar cells.[1] Additional research areas include morphology,[2,4] processing,[6] manufacturing,[11,12] and demonstration of the technology.

The most studied polymer solar cell employs morphologically stable bulk heterojunctions of regioregular P3HT (Figure 1) as the donor material and the fullerene material PCBM (Figure 1) as the acceptor material. P3HT:PCBM based devices are

(1) Jørgensen, M.; Norrman, K.; Krebs, F. C. *Sol. Energy Mater. Sol. Cells* **2008**, *92*, 686–714.
(2) Thompson, B. C.; Fréchet, J. M. J. *Angew. Chem., Int. Ed.* **2008**, *47*, 58–77.
(3) Günes, S.; Sariciftci, N. S. *Inorg. Chim. Acta* **2008**, *361*, 581–588.
(4) Hoppe, H.; Sariciftci, N. S. *Adv. Polym. Sci.* **2008**, *214*, 1–86.
(5) Saunders, B. R.; Turner, M. L. *Adv. Colloid Interface Sci.* **2008**, *138*, 1–23.
(6) Krebs, F. C. *Sol. Energy Mater. Sol. Cells* **2009**, *93*, 394–412.
(7) Ameri, T.; Dennler, G.; Lungenschmied, C.; Brabec, C. J. *Energy Environ. Sci.* **2009**, *2*, 347–363.
(8) Kippelen, B.; Brédas, J. L. *Energy Environ. Sci.* **2009**, *2*, 251–261.
(9) Peet, J.; Heeger, A. J.; Bazan, G. *Acc. Chem. Res.* **2009**, *42*, 1700–1708.
(10) Gonzalez-Valls, I.; Lira-Cantu, M. *Energy Environ. Sci.* **2009**, *2*, 19–34.
(11) Krebs, F. C.; Gevorgyan, S. A.; Alstrup, J. *J. Mater. Chem.* **2009**, *19*, 5442–5451.
(12) Krebs, F. C.; Norrman, K. *ACS Appl. Mater. Interfaces* **2010**, *2*, 877–887.
(13) Park, S. H.; Roy, A.; Beaupré, S.; Cho, S.; Coates, N.; Moon, J. S.; Moses, D.; Leclerc, M.; Lee, K.; Heeger, A. J. *Nat. Photonics* **2009**, *3*, 297–303.
(14) Chen, H. Y.; Hou, J.; Zhang, S.; Liang, Y.; Yang, G.; Yang, Y.; Yu, L.; Wu, Y.; Li, G. *Nat. Photonics* **2009**, *3*, 649–653.
(15) Katz, E. A.; Gevorgyan, S.; Orynbayev, M. S.; Krebs, F. C. *Eur. Phys. J. Appl. Phys.* **2006**, *36*, 307–311.
(16) Hauch, J. A.; Schilinsky, P.; Choulis, S. A.; Childers, R.; Biele, M.; Brabec, C. J. *Sol. Energy Mater. Sol. Cells* **2008**, *92*, 727–731.
(17) Krebs, F. C. *Sol. Energy Mater. Sol. Cells* **2008**, *92*, 715–726.
(18) Zimmermann, B.; Würfel, U.; Niggemann, M. *Sol. Energy Mater. Sol. Cells* **2009**, *93*, 491–496.

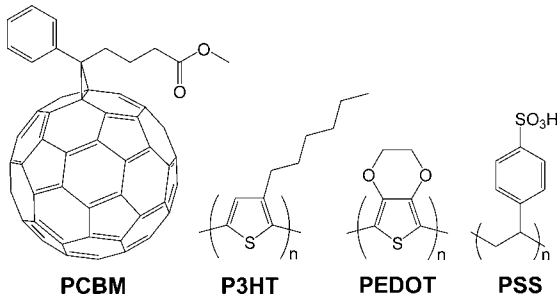

Figure 1. Organic materials used in this work. [6,6]-Phenyl-C61-butyric acid methyl ester (PCBM) is the acceptor material, poly(3-hexylthiophene) (P3HT) is the donor material, and the mixture of the ionomers poly(3,4-ethylenedioxythiophene) (PEDOT) and poly(styrenesulfonate) (PSS) forms the PEDOT:PSS material that acts as a hole transport layer.

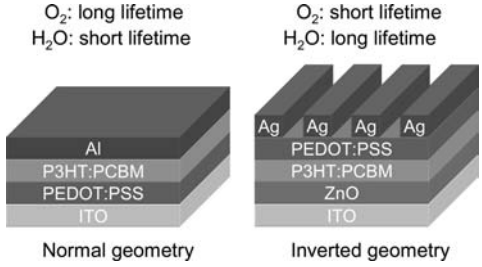

Figure 2. Schematics of a device with normal geometry (left) and a device with inverted geometry (right). The substrate that may be glass or poly(ethylene terephthalate) (PET) is not shown. The thicknesses of the layers are exaggerated for clarity.

typically prepared by simple solution processing of the active layers followed by evaporation of metallic back electrodes, which produces a device with a so-called "normal" geometry where electrons flow from the transparent electrode to the back electrode (Figure 2). A normal geometry is convenient when preparing devices on a lab scale but undesirable for a large-scale production due to the vacuum processing steps. As a result, so-called "inverse" or "inverted" device geometries where electrons flow from the back electrode to the transparent electrode (Figure 2) were developed that allow for the use of a solution processed back electrode.[11,19] With inverse geometry devices, vacuum processing can thus be avoided (except for the ITO electrode). Preliminary demonstrations of large-scale manufacturing of inverse geometry devices show feasibility and confirm the advantages of an inverse geometry. However, more work is needed to further optimize the inverse geometry devices such that the large-scale vision for the polymer solar technology can be realized.

This work focuses on device lifetime. To optimize the device lifetime, one needs to understand how the device degrades during operation. The limited lifetime is a result of several processes that are in play simultaneously. Materials degrade and as a consequence so do in many instances their physical, electrical, and mechanical properties. Photovoltaic devices that rely on the delicate interplay between the electronic structure of the material, and the energy levels in external electrodes connecting the functional material in the device to the outside world, are highly sensitive to even small degrees of degradation. For an electronic device based on organic materials that rely on both bulk and interface phenomena, it is clear that degradation becomes highly critical for device function and thus must be removed or at least minimized to improve stability. Degradation comprises a complex range of mechanisms of which presumably not all have been identified. Known degradation mechanisms involve: diffusion of molecular oxygen and water into the device, degradation of interfaces, degradation of the active material, interlayer and electrode diffusion, electrode reaction with the organic materials, morphological changes, and macroscopic changes such as delamination, formation of particles, bubbles, and cracks. Some of these degradation mechanisms are interrelated and take place at the same time, some during operation of the solar cell, and some during storage. Some degradation mechanisms are fast, and others are slow. It is thus a challenging task to identify degradations mechanisms, and even more difficult to quantify to what extent each mechanism contributes to the overall deterioration of the solar cell performance. It has been known for a long time that diffusion of molecular oxygen and water into the device leads to some of the most significant degradation mechanisms for organic solar cells. In this work, we seek a more detailed understanding of this phenomenon.

Earlier work from this laboratory has shown that, for normal geometry devices using aluminum as a back electrode, both molecular oxygen and water will diffuse through the aluminum electrode.[11,20−24] Molecular oxygen will preferentially diffuse through microscopic pinholes in the electrode, and water will preferentially diffuse in between the aluminum grains in the electrode. Both molecular oxygen and water will then diffuse through all the layers in the device all the way to the ITO interface. All organic layers will react with molecular oxygen and water in varying degree causing oxidation and thus degradation. At the ITO interface, oxygen from the ITO will be exchanged with the incoming oxygen (i.e., in the form of molecular oxygen and water). These processes are in varying degree affected by light and/or heat. Degradation takes place even during storing but to a lesser degree; that is, the devices will not have an infinite shelf lifetime.

Switching from lab-scale (i.e., normal geometry) to large-scale manufacturing made it relevant to perform the same lifetime experiments on an inverted geometry device. The inverted geometry device shown in Figure 2 was lifetime tested thoroughly with an interesting result.[11] Whereas the normal geometry device (Figure 2) was shown to have a relatively long lifetime in an O_2:N_2 (1 atm) atmosphere and a relatively short lifetime in a saturated H_2O atmosphere, the inverted geometry device showed the opposite behavior, that is, short lifetime in O_2:N_2 (1 atm) and a long lifetime in saturated H_2O.[11] The observation of a relatively good stability in separate water and oxygen atmospheres gave hope that devices stable in the presence of both water and oxygen could be made, and initially the search for the instability in oxygen for the inverted devices was sought at the metal PEDOT:PSS interface. The use of many

(19) Waldauf, C.; Morana, M.; Denk, P.; Schilinsky, P.; Coakley, K.; Choulis, S. A.; Brabec, C. J. *Appl. Phys. Lett.* **2006**, *89*, 233517.
(20) Gevorgyan, S. A.; Jørgensen, M.; Krebs, F. C. *Sol. Energy Mater. Sol. Cells* **2008**, *92*, 736–745.
(21) (a) Norrman, K.; Krebs, F. C. *Sol. Energy Mater. Sol. Cells* **2006**, *90*, 213–227. (b) Seemann, A.; Egelhaaf, H.-J.; Brabec, C. J.; Hauch, J. A. *Org. Electron.* **2009**, *10*, 1424–1428. (c) Manceau, M.; Rivaton, A.; Gardette, J. L.; Guillerez, S.; Lemaitre, N. *Polym. Degrad. Stab.* **2009**, *94*, 898–907.
(22) (a) Norrman, K.; Gevorgyan, S. A.; Krebs, F. C. *ACS Appl. Mater. Interfaces* **2009**, *1*, 102–112. (b) Hauch, J. A.; Schilinsky, P.; Choulis, S. A.; Rajoelson, S.; Brabec, C. J. *Appl. Phys. Lett.* **2008**, *93*, 103306.
(23) Norrman, K.; Larsen, N. B.; Krebs, F. C. *Sol. Energy Mater. Sol. Cells* **2006**, *90*, 2793–2814.
(24) Norrman, K.; Alstrup, J.; Krebs, F. C. *Surf. Interface Anal.* **2006**, *38*, 1302–1310.

printed metal electrodes different from silver (Mo, Cr, Ti, and Au) did not remove/solve the problem, and silver remained the best printable electrode material. It should be noted that evaporated metal electrodes based on Cr, Ti/Au, and Cu have been reported.[25−27] The assumption that the PEDOT:PSS−active layer interface was an invariant was natural because that interface works quite well in oxygen for normal geometry devices. The only difference between the PEDOT:PSS−active layer interface in normal and inverted devices is the order in which it is processed, the processing itself, and also the nature of the PEDOT:PSS. In devices with a normal geometry, the PEDOT:PSS−active layer interface is created by coating a solution of the active layer on the surface of a solid PEDOT:PSS film. PEDOT:PSS has a large surface energy, and the active layer solution in chlorobenzene has a low surface tension and wets the PEDOT:PSS film well. In contrast to this, devices with an inverted geometry are prepared by coating a dispersion of PEDOT:PSS that typically presents a high surface tension onto the surface of a solid active-layer film that typically presents a relatively low surface energy. To overcome this, isopropanol is used to wet the solid active-layer surface and is also added to the PEDOT:PSS dispersion to lower the surface tension. This initiated a quest to gain more detailed information on the relative effects of molecular oxygen and water on polymer solar cells. In addition, previous studies employed an experimental approach that made it possible to detect whether molecular oxygen and water had reacted with the device components or not.[20−24] However, it was not possible quantitatively to measure the extent of oxygen that reacted with the components, as only limited semiquantitative information was available. In this work, we have modified the experimental procedures such that quantitative information is available. Systematic experiments have been performed on the inverse geometry device shown in Figure 2. The results are reported herein.

Some recent publications deal with issues that are relevant for this work.[21,28−30] Seemann et al.[21b] studied degradation behavior of an inverted device similar to the one described in Figure 2. They found that due to the gas permeability of the PEDOT:PSS, oxygen can diffuse through, which, combined with illumination, results in a strong decrease of the short circuit current (within minutes). The authors explain the decrease from a change in the conductivity of the PEDOT:PSS layer, and they found that the short circuit current can be partially recovered by heating, which they take as an indication of degradation taking place in the photoactive layer. Yamanari et al.[30] studied the effect of PEDOT:PSS in a normal geometry device with respect to degradation. It was found that when PEDOT:PSS is used degradation is fast as compared to either no PEDOT:PSS or using MoO_x instead of PEDOT:PSS. They showed that PEDOT:PSS accelerates the formation of aluminum oxide in the interface between the aluminum electrode and the active layer.

Table 1. Photovoltaic Parameters for the Batch of Solar Cell Devices That Were Tested in the Ambient Atmosphere Measured Prior to the Degradation Experiment (25 ± 5% Relative Humidity, 72 ± 2 °C) Using AM1.5G Illumination (1000 W m^{-2})[a]

device type	J_{sc} (mA cm^{-2})	V_{oc} (V)	FF	PCE (%)
not encapsulated	−8.4 ± 2.5	0.54 ± 0.02	39 ± 4	1.79 ± 0.4
encapsulated	−7.9 ± 1.5	0.52 ± 0.01	43 ± 2	1.78 ± 0.3

[a] The device configuration is ITO−ZnO−P3HT:PCBM−PEDOT:PSS−printed silver. Average values are shown with corresponding standard deviations (3 cm^2 active area).

Results and Discussion

Experimental Approach. To clarify the experiments involved in this project, the setup is briefly described. Three sets of samples were prepared: one set acted as reference samples and were stored in a glovebox (1 atm N_2, 20 ± 2 °C, darkness); the two other sets were each placed in separate chambers equipped with a quartz window allowing illumination (330 W m^{-2}, 65 ± 2 °C), and a dry atmosphere consisting of $^{18}O_2$:N_2 (1 atm, 0% rh), or a humid atmosphere consisting of $H_2{}^{18}O$ (1 atm N_2, < 1 ppm O_2, 65% rh). Each set of samples consisted of two devices of which one was wrapped in aluminum foil (i.e., only exposed to the heat and the atmosphere), and one was not. Both encapsulated and nonencapsulated devices were studied.

***IV*-Characteristics and Degradation.** Table 1 presents the key photovoltaic parameters for the batch of solar cell devices that were tested in the ambient atmosphere (25 ± 5% rh, 72 ± 2 °C) using a xenon lamp that provided AM1.5G illumination (1000 W m^{-2}), and Figure 3 shows the evolution of the solar cell parameters as a function of time during the degradation experiments in the presence of isotopically labeled water or oxygen.

The current state-of-the-art performance reported for small area (mm^2) devices based on P3HT−PCBM is higher than the performance for the devices studied here. It should, however, be stressed that our devices employ larger area (3 cm^2), printed metal electrodes, and a device geometry that is fully roll-to-roll (R2R) compatible. The decrease in going from the lab-scale device, through larger area to printed electrodes and R2R processing, has been detailed earlier.[11] A technicality of the experiment is that the devices need to be mounted in an atmosphere chamber,[20] which involves gluing the devices onto a sample holder, and mounting them in the atmosphere chamber, with subsequent exchange of the atmosphere with the desired isotopically labeled atmosphere (either dry oxygen or humid nitrogen). This procedure took around 1 h and led to slight degradation of the device performance. In terms of the interpretation of the degradation of the devices, both encapsulated and nonencapsulated devices were tested under each condition as shown in Figure 3. It is clear that the nonencapsulated devices are adversely affected by the surrounding atmosphere, and the encapsulated devices perform quite well with only slight degradation over the course of the experiment during which the illumination was continuous. The encapsulated devices represent the device in a form where it could be embodied in an application.

In such cases, the lifetime or end of life for the device is often quoted as the T80 or T50, which, respectively, is the time it takes for a device to reach 80% or 50% of the initial

(25) Zimmermann, B.; Würfel, U.; Niggemann, M. *Sol. Energy Mater. Sol. Cells* **2009**, *93*, 491–496.
(26) Zimmermann, B.; Glatthaar, M.; Niggemann, M.; Riede, M. K.; Hinsch, A.; Gombert, A. *Sol. Energy Mater. Sol. Cells* **2007**, *91*, 374–378.
(27) Reeja-Jayan, B.; Manthiram, A. *Sol. Energy Mater. Sol. Cells* **2010**, *94*, 907–914.
(28) Takayuki Kuwabara, T.; Iwata, C.; Yamaguchi, T.; Takahashi, K. *ACS Appl. Mater. Interfaces* **2010**, *2*, 2254–2260.
(29) Lira-Cantu, M.; Siddiki, M. K.; Muñoz-Rojas, D.; Amade, R.; González-Pech, N. I. *Sol. Energy Mater. Sol. Cells* **2010**, *94*, 1227–1234.
(30) Yamanari, T.; Taima, T.; Sakai, J.; Tsukamoto, J.; Yoshida, Y. *Jpn. J. Appl. Phys.* **2010**, *49*, 01AC02.

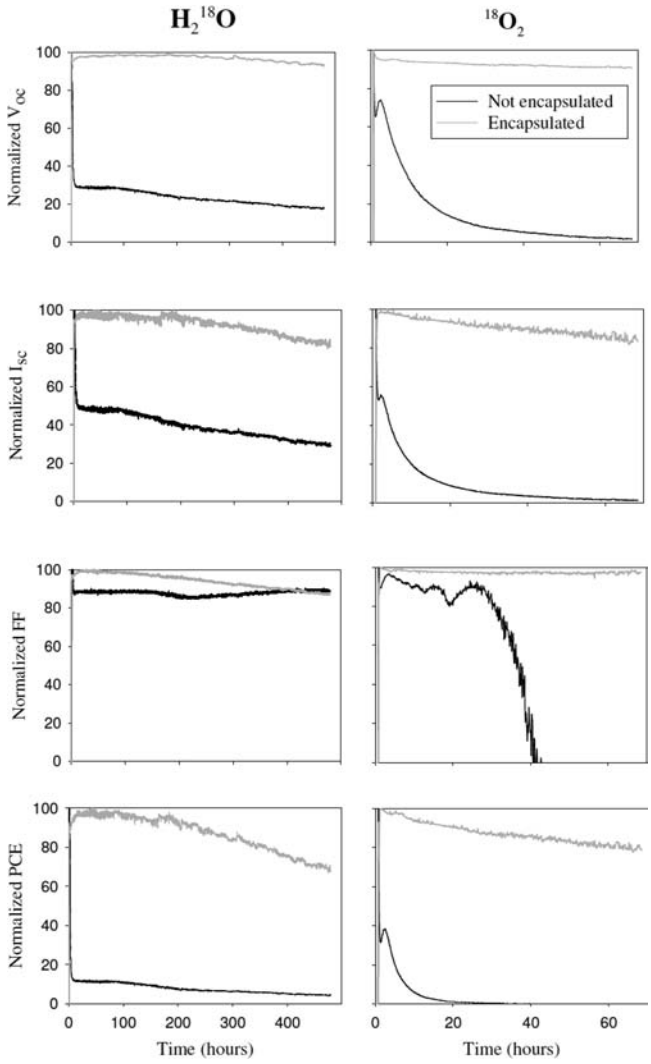

Figure 3. Degradation of encapsulated and nonencapsulated devices under continuous illumination (330 W m^{-2}, AM1.5G, 65 ± 2 °C) in an oxygen-free isotopically labeled humid atmosphere (65 ± 2% rh, left) or in a dry (<0.1% rh) isotopically labeled oxygen atmosphere (20% $^{18}O_2$, 80% N_2, right).

performance. The T80 for the encapsulated devices in respectively water and oxygen containing atmospheres was 360 and 68 h. In the absence of encapsulation, both atmospheres lead to fast degradation of the initial response with T80/T50 of, respectively, 1.9/2.2 h in water and 0.1/0.3 h in oxygen. The oxygen atmosphere led to complete and irreversible degradation of the device in less than 20 h with all parameters showing fast decay. After approximately 25 h, the performance was zero, and the data became very noisy. The voltage and current decreased exponentially. In the humid atmosphere, device performance decreased by a factor of 10 during the first 10 h, and then stabilized at a roughly constant level for the remaining part of the experiment, which was arrested after 480 h. In the humid atmosphere, the FF stays essentially constant, while both the voltage and the current drop to a lower level. On the basis of the findings (vide supra), we ascribed this to absorption/desorption of water in the PEDOT:PSS layer that adversely affected the performance, and we assumed that the observed changes in performance were due to poor transport at the PEDOT:PSS interfaces and in the bulk of PEDOT:PSS. Simple experiments on model PEDOT:PSS films showed significant variation in conductivity/resistance as a function of humidity level, thus confirming the humidity dependence (see the Supporting Information). To further shed light on this observation, experiments were carried out on complete devices under the same conditions of illumination and low oxygen content, while varying the relative humidity (using normal $H_2{}^{16}O$) in steps between <1% rh and ~40% rh (330 W m^{-2}, 65 ± 2 °C). This showed that a low humidity adversely affected the device performance. The effect was found to be reversible, and most significant for the V_{oc} (see Figure S1 in the Supporting Information). Both FF and I_{sc} are less affected and exhibit a fast and reversible response relatively independent of changes in relative humidity, and we ascribe changes in these parameters to be due to changes in transport properties for the PEDOT:PSS−active layer interface (see the Supporting Information). When a change in voltage is observed, it is most often due to a change in the band edges for the materials at the interface. Possible mechanisms that could account for our observation are thus a reorganization of molecules at the interface that lead to a change in the effective work function of PEDOT:PSS by affecting either the carrier density in PEDOT:PSS near the interface or the formation of a dipole layer at the interface. It is likely that both mechanisms are in play. It is also noteworthy that in Figure 3, where the lifetime experiment was performed on devices that were exposed to humidity, only during preparation exhibited a fast stabilization of V_{oc} (in about 10 h), which concurs with the first cycle in Figure S1 (see the Supporting Information). However, the stabilization period upon reducing humidity in Figure S1 becomes slower with every cycle. The recovery of the device upon increasing the humidity level from <1% rh to 40% rh is fast in every case. This can possibly be viewed as a slow drying of the PEDOT:PSS and fast water uptake. What is interesting is, however, that both I_{sc} and FF react so quickly to the changes and thus confirm that it is unlikely to be due to a change in the bulk conductivity of PEDOT:PSS alone. It could, however, be associated with a gradual increase in the barrier to charge transport across the PEDOT:PSS−active layer interface as water is dried out of the PEDOT:PSS. This led to a careful and systematic elucidation of where, respectively, water and oxygen react in the dark and under illumination in complete devices and reference films of the materials.

Quantifying the Accumulated Oxygen Uptake during Operation of the Device. One of the goals of this work was to quantify how much chemically bound oxygen that was introduced as a result of exposure to water or molecular oxygen. In previous work, time-of-flight secondary ion mass spectrometry (TOF-SIMS) was used as the chemical characterization technique. However, TOF-SIMS is not directly quantitative (only semiquantitative in certain situations), so X-ray photoelectron spectrometry (XPS) being a quantitative chemical characterization technique was chosen.

To ascertain what kind of information can be extracted from an XPS analysis of the devices in question, a test experiment was performed. The samples glass-P3HT, glass-PCBM, and glass-PEDOT:PSS were subjected to illumination (1000 W m^{-2}, 72 ± 2 °C) in ambient air (25 ± 5% rh), and XPS spectra were obtained as a function of time. Two types of information were acquired: (i) element compositions and (ii) high-resolution peak shapes that, among other things, contain chemical state information. Figure 4 shows the oxygen uptake relative to no illumination as a function of time. As expected, the oxygen content is observed to increase with time for P3HT and PCBM. However,

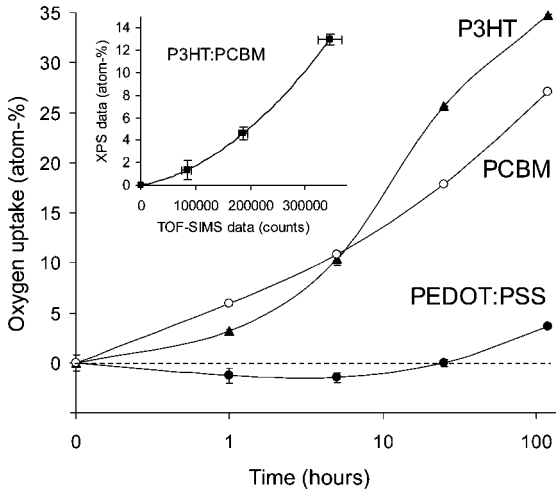

Figure 4. Oxygen uptake in atom % for spin-coated films of P3HT, PCBM, and PEDOT:PSS as a result of illumination (1000 W m^{-2}, 72 ± 2 °C) in ambient air (25 ± 5% rh). The corresponding plot for P3HT:PCBM is not shown for clarity. The horizontal dashed line represents 0 atom %. The inset is XPS data calibrated against TOF-SIMS data for P3HT:PCBM. Each point is an average of five measurements on different surface locations.

for PEDOT:PSS the oxygen content initially decreases, and then later on it starts to increase. This is attributed to the occurrence of one or more mechanisms taking place at the same time; that is, the material is both gaining and loosing oxygen, and initially the oxygen loss outweighs the oxygen gain. It is not possible to explain this phenomenon in more detail because PEDOT:PSS is a commercial material containing one or more unknown additives. It should be noted that the probe depth of XPS is very limited (5−10 nm), so the results are not representative of the bulk material; that is, the material itself acts as a barrier so a smaller degree of oxidation is expected in the bulk of the film.

Figure 5 displays high-resolution S_{2p} and C_{1s} XPS spectra for P3HT for the experiment presented in Figure 4. The binding energies of the core electrons in elements are slightly influenced by the chemical surrounding including the chemical state. This phenomenon is manifested in a slight shift in the peak position, a so-called chemical shift. In Figure 5a, peak broadening is observed for the S_{2p} peak, which is ascribed to chain scissions between the thiophene units in the polymer backbone, or (more likely) loss of the side chains. At longer exposure times, the aromatic bonds will most likely be broken, enabling $R-SO_X$ species to be formed. In the C_{1s} spectra (Figure 5b), peaks from oxygenated carbon species are emerging, in particular, the R−COOH peak.

As is evident from Figures 4 and 5, it is possible to use XPS to monitor the chemical changes that take place in the outer 5−10 nm of the surface during illumination in an ambient atmosphere with some specificity. The next step is to perform the same XPS analyses on the devices that were exposed to illumination in the controlled atmospheres ($^{18}O_2$:N_2 and $H_2{}^{18}O$:N_2), together with the device that was stored in the glovebox (darkness, N_2). Table 2 lists the measured oxygen contents for the devices at two surfaces (Figure S5). Surprisingly, there is no detectable difference in oxygen contents between the device that was stored in darkness in N_2 and the devices that were illuminated in dry $^{18}O_2$:N_2 or oxygen free $H_2{}^{18}O$:N_2 if the uncertainty (i.e., point-to-point variation) is taken into account. The theoretical calculated oxygen content is ∼3 atom % lower than what is measured at the PEDOT:PSS surface, and ∼2 atom % lower than what is measured on the P3HT:PCBM surfaces.

This is ascribed to possible reaction with molecular oxygen and/or water during handling and fabrication. For PEDOT:PSS, there could, in addition, be an oxygen contribution from the unknown additives. Figure 6 shows the corresponding high-resolution C_{1s} and S_{2p} XPS spectra for the P3HT:PCBM surfaces, which support the findings presented in Table 2. No detectable S_{2p} peak broadening (presumably indicative of bond breaking) is observed, and only a minor degree of oxygenated carbon species is observed as a result of illumination in $^{18}O_2$:N_2 or $H_2{}^{18}O$. The lack of a small R−COOH peak (from PCBM) for the device that was stored in darkness in N_2 can be explained by P3HT enrichment at the P3HT:PCBM−PEDOT:PSS interface, which is a well-documented phenomenon.[31−33]

The results presented in Table 2 and Figure 6 are very interesting because they suggest that during the lifetime of the device the extent of chemical degradation is on a scale that is either lower than the detection level of XPS or lower than the accuracy of the measurement determined by the point-to-point variations on the surfaces. In conclusion, XPS is not sensitive and/or accurate enough to measure the apparent small amount of oxygen uptake resulting from illuminating the device in dry $^{18}O_2$:N_2 or oxygen free $H_2{}^{18}O$:N_2. XPS provides quantitative information but lacks sufficient sensitivity, and TOF-SIMS is not directly quantitative, but is extremely sensitive. The obvious thing to do is to combine the data from the two techniques. The samples from the test experiment where the individual materials were illuminated as a function of time in ambient air and subsequently XPS analyzed (Figure 4) were, in addition, analyzed with TOF-SIMS. TOF-SIMS-acquired ^{16}O peak intensities (in counts) were correlated with XPS acquired oxygen intensities (in atom %), resulting in calibration plots. The inset in Figure 4 shows the calibration plot for P3HT:PCBM. By extrapolating, it is possible to transform the nonquantitative TOF-SIMS data into quantitative data. This is very useful because the ^{16}O signal from a TOF-SIMS measurement cannot be compared for different materials due to a possible/likely matrix effect. It should be noted that because an extrapolation is used an additional error could be introduced, which is difficult to determine. With the XPS calibrated data, it is now possible to quantitatively compare low-level oxygen contents for different materials. This procedure can now be used to quantify the oxygen uptake in the devices that were exposed to an $^{18}O_2$:N_2 or a $H_2{}^{18}O$ atmosphere. The advantage of using a mass spectrometry-based technique (TOF-SIMS) in conjunction with $^{18}O_2$ or $H_2{}^{18}O$ is the ability to specifically measure the oxygen uptake that occurred during the experiment only. By measuring the ^{18}O signal, one disregards the oxygen (^{16}O) coming from the material itself or from oxidation during handling and fabrication. Natural oxygen contains 0.2% ^{18}O, which is easily compensated for by measuring the ^{16}O signal intensity. Figure 7 shows the oxygen uptake for four devices (with no encapsulation) that were exposed to dry $^{18}O_2$:N_2 or oxygen free $H_2{}^{18}O$:N_2, of which two of them were wrapped in aluminum foil

(31) Chen, L.-M.; Hing, Z.; Li, G.; Yang, Y. *Adv. Mater.* **2009**, *21*, 1434–1449.
(32) van Bavel, S.; Sourty, E.; de With, G.; Frolic, K.; Loos, J. *Macromolecules*, DOI:10.1021/ma900817t.
(33) Xu, Z.; Chen, L.-M.; Yang, G.; Huang, C.-H.; Hou, J.; Wu, Y.; Li, G.; Hsu, C.-S.; Yang, Y. *Adv. Funct. Mater.* **2009**, *19*, 1227–1234.
(34) Andersen, M.; Carlé, J. E.; Cruys-Bagger, N.; Lilliedal, M. R.; Hammond, M. A.; Winther-Jensen, B.; Krebs, F. C. *Sol. Energy Mater. Sol. Cells* **2007**, *91*, 539–543.

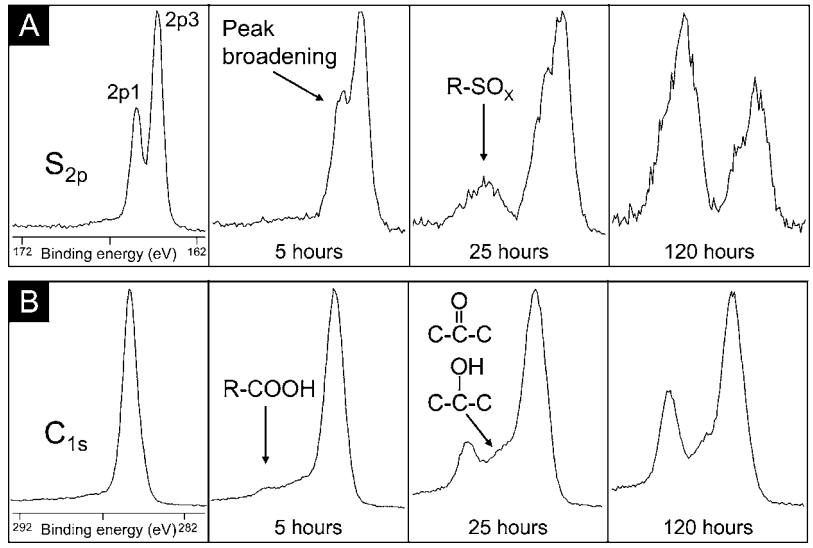

Figure 5. High-resolution S_{2p} and C_{1s} XPS spectra of P3HT for various exposure times (1000 W m^{-2}, 72 ± 2 °C) in ambient air (43 ± 5% rh). The first spectrum in each row represents 0 h (no illumination). The intensity has been normalized in each spectrum for clarity.

Table 2. XPS Measured Oxygen Contents for Devices Exposed to Different Conditions[a]

analyzed surface	theoretical (atom %)	stored in darkness in N_2 (atom %)	illuminated in $^{18}O_2$:N_2 (atom %)	illuminated in $H_2{}^{18}O$ (atom-%)
PEDOT:PSS	23.8	27.0 ± 0.4	26.7 ± 2.3	26.5 ± 0.3
P3HT:PCBM	2.4	5.1 ± 2.1	3.9 ± 0.3	4.8 ± 1.7

[a] The PEDOT:PSS surface was analyzed between the silver stripes (Figure S5), and the P3HT:PCBM surface was analyzed after removal of the PEDOT:PSS layer (Figure S5). Each value is an average of five measurements on different surface locations.

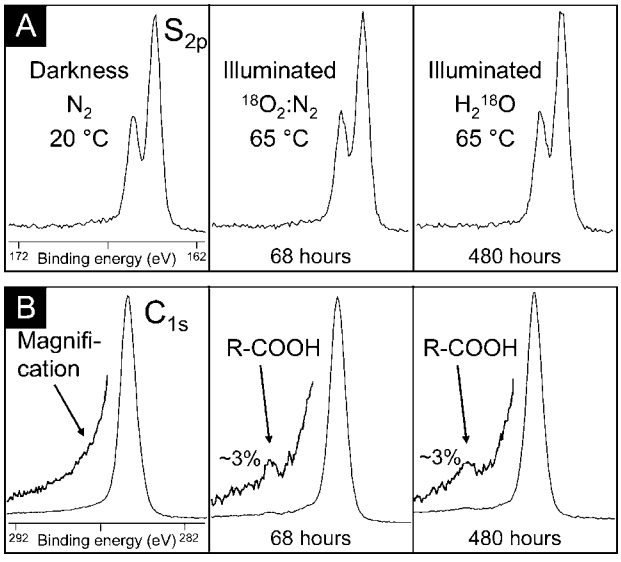

Figure 6. High-resolution S_{2p} and C_{1s} XPS spectra of the P3HT:PCBM surface for three devices exposed to different conditions. The ~3% corresponds to the area ratio between the R−COOH peak and the remaining C_{1s} peak. The durations of the illumination of the devices are shown below each spectrum. The intensity has been normalized in each spectrum for clarity. Illumination conditions were 1000 W m^{-2}, 72 ± 2 °C, AM1.5G.

(darkness) and two of them were illuminated. It should be emphasized that these results corresponds to the outer 5−10 nm of the film corresponding to the probe depth; that is, the results are not representative of the bulk of the film. On the basis of Figure 7, it is now possible to compare the data in

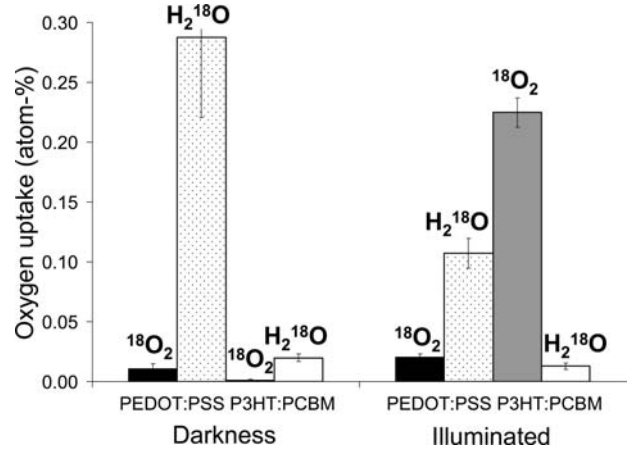

Figure 7. Oxygen uptake measured by XPS calibrated TOF-SIMS data for the devices. "Darkness" corresponds to the devices that were wrapped in aluminum foil and stored together with the illuminated devices in a dry $^{18}O_2$:N_2 or an oxygen free $H_2{}^{18}O$:N_2 atmosphere; that is, all devices were exposed to the heat and the atmosphere. Each value is an average of five measurements on different surface locations. Illumination conditions were 330 W m^{-2}, 65 ± 2 °C, AM1.5G.

various ways. PEDOT:PSS reacts relatively efficiently with water, which is probably related to the fact that PEDOT:PSS is soluble in water. However, PEDOT:PSS reacts less with water during illumination. A possible explanation could be that the devices wrapped in aluminum foil have a temperature similar to that of the surrounding chamber during the experiment, and the illuminated devices have a slightly higher temperature due to the illumination. This would decrease the contact with water for the slightly heated devices and decrease the reactivity. The same phenomenon is to a minor degree observed for P3HT:PCBM exposed to water. Furthermore, PEDOT:PSS is observed to be relatively resilient toward molecular oxygen. P3HT:PCBM reacts relatively efficiently with molecular oxygen when illuminated but close to not at all when stored in darkness. At first it would seem that the worst situation in regard to degradation is PEDOT:PSS reacting with water. However, one should consider that the device that was illuminated in water had the better stability, that is, 360 h as compared to 68 h with respect to T80. Thus, the most serious situation in regard to

degradation must be P3HT:PCBM reacting with molecular oxygen during illumination. Another thing to consider is the fact that the P3HT:PCBM surface (i.e., the P3HT:PCBM−PEDOT:PSS interface) is protected by the PEDOT:PSS layer that acts as a poor barrier layer against water and molecular oxygen. The PEDOT:PSS surface, on the other hand, is, because of the silver electrode grid pattern, exposed directly to the atmosphere. This should be considered when comparing the results. It was unfortunately not possible to expose the PEDOT:PSS surface that is located under the silver electrode.

It is difficult to relate the result from Figure 7 to the overall deterioration of solar cell performance. It is unknown whether many mechanisms contribute or one mechanism acts as a bottleneck. The fact that only extremely low levels of material react with molecular oxygen and water during the device lifetime suggests that the dominating factor, with respect to deterioration of solar cell performance, most likely is an interface phenomenon, which is especially vulnerable, because only a small degree of degradation can profoundly impede the electrical transport properties. If the device lifetime is related to reaction of water and molecular oxygen at the interfaces, is it then possible to explain why the normal geometry device (Figure 2) exhibits an opposite behavior with respect to lifetime and atmosphere? The relatively short lifetime for the normal geometry device (ITO−PEDOT:PSS−P3HT:PCBM−Al) in a water atmosphere could be related to the aluminum electrode. We have previously shown[22a] that water diffuses through the aluminum grains, a process that unavoidably will lead to the formation of aluminum hydroxide/oxide, which is an insulator. Molecular oxygen preferentially diffuses through pinholes in the electrode that could be a slower diffusion mechanism as compared to diffusion of water in between the aluminum grains. We have shown that P3HT:PCBM is relatively vulnerable toward molecular oxygen during illumination. For the inverse geometry device (ITO−ZnO−P3HT:PCBM−PEDOT:PSS−Ag), PEDOT:PSS acts as a protecting barrier for the P3HT:PCBM−PEDOT:PSS interface with respect to water and molecular oxygen. For the normal geometry device, aluminum acts as a weak barrier for the P3HT:PCBM. If degradation of the P3HT:PCBM interfaces is related to the lifetime, then one could speculate that aluminum is a better barrier as compared to PEDOT:PSS with respect to molecular oxygen. Especially the reactivity of aluminum toward dry oxygen is very low, as shown earlier in the case of a low band gap polymer.[35] The reaction of the aluminum interface is assumed to be similar to calcium, for which it has been shown that the interface is stable in the presence of dry oxygen, but will degrade quickly in the presence of water.[36]

In-Depth Mapping of Water and Molecular Oxygen-Induced Degradation. The ZnO surface (i.e., the P3HT:PCBM−ZnO interface) was not included in the previous discussions regarding quantification of the oxygen uptake during exposure to a dry $^{18}O_2$:N_2 or an oxygen free $H_2{}^{18}O$:N_2 atmosphere. The reason is that the TOF-SIMS ^{16}O signals obtained from the ZnO surfaces were all extremely saturated, which made it impossible to compensate for the natural ^{18}O isotope ($^{18}O/^{16}O = 0.2\%$) that consequently contributed significantly.

Alternatively, TOF-SIMS depth profiling was employed, which suffers from the fact that XPS cannot be implemented, so the study is only semiquantitative. The sputter process part of the depth profiling procedure drastically reduces the sensitivity, which is an advantage when dealing with otherwise saturated signals. The two nonencapsulated devices that were illuminated in dry $^{18}O_2$:N_2 or oxygen free $H_2{}^{18}O$:N_2 atmospheres were subjected to TOF-SIMS depth profiling analyses to map the in-depth degradation caused by water or molecular oxygen. Both devices were analyzed starting from the P3HT:PCBM surfaces (Figure S5) to optimize the depth resolution, which deteriorates for longer sputter times. Both devices resulted in depth profiles that were identical with respect to P3HT, PCBM, ZnO, and ITO. These profiles are shown in Figure 8 for the device that was illuminated in a dry $^{18}O_2$:N_2 atmosphere. The corresponding profiles for the device that was stored in a glovebox were identical (not shown).

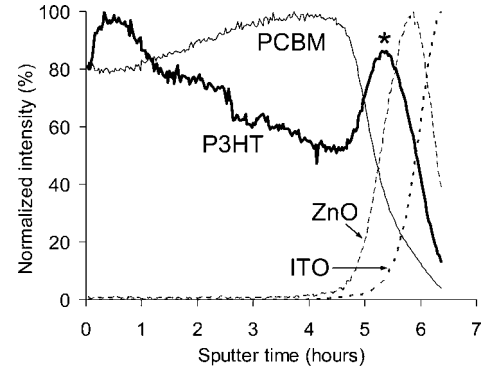

Figure 8. TOF-SIMS depth profiles (starting from the P3HT:PCBM surface, Figure S5) for the device that was illuminated in a dry $^{18}O_2$:N_2 atmosphere. The markers used are: S^- (P3HT), C_3^- (PCBM, with a possible contribution from P3HT), ZnO_2^- (ZnO), and InO_2^- (ITO). The profiles were normalized against the total intensity to remove possible instrument effects. The asterisk points to an intensity optimum that indicates an extreme matrix effect and/or a P3HT enrichment at the P3HT:PCBM interface.

The P3HT and the PCBM profiles (Figure 8) reveal a well-known phenomenon (not related to degradation). As a result of the spin-coating process (of P3HT:PCBM onto ZnO), P3HT is enriched at the upper surface that is exposed to air after spin coating. This is observed in Figure 8 as a decrease in the P3HT signal and an increase in the PCBM signal for longer sputter times (i.e., in depth). The profiles in Figure 8 are normalized against the total ion intensity to remove possible instrument effects. The P3HT intensity optimum indicated by the asterisk suggests either P3HT enrichment at the P3HT:PCBM−ZnO interface and/or an extreme matrix effect that is not adequately compensated for by the normalization procedure. Figure 9 displays the same PCBM and ZnO profiles that are presented in Figure 8, along with $^{18}O/^{16}O$ intensity ratio profiles for the devices that were exposed to a dry $^{18}O_2$:N_2 or an oxygen free $H_2{}^{18}O$:N_2 atmosphere. As an alternative to nonavailable quantitative ^{18}O information, the $^{18}O/^{16}O$ ratio was monitored. However, this requires a comment or two. Because the two devices have the same configuration, the ratio profiles can be compared directly (semiquantitatively). However, the $^{18}O/^{16}O$ ratio cannot be semiquantitatively compared within the same profile for sputter time windows corresponding to different materials, that is, for P3HT:PCBM and ZnO. There are two reasons for this: (i) different materials are expected, due to a possible matrix effect, to exhibit different response factors (in this case for oxygen), and (ii) ZnO contains 50% oxygen (if possible residues from the organic derivative, used to make it soluble, are disregarded), which will contribute significantly to the $^{18}O/^{16}O$ ratio.

(35) Petersen, M. H.; Gevorgyan, S. A.; Krebs, F. C. *Macromolecules* **2008**, *41*, 8986–8994.
(36) Cros, S.; Firon, M.; Lenfant, S.; Trouslard, P.; Beck, L. *Nucl. Instrum. Methods Phys. Res., Sect. B* **2006**, *251*, 257–260.

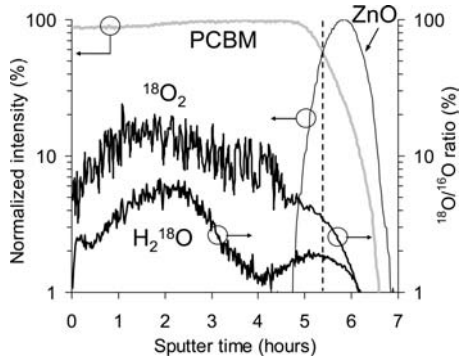

Figure 9. TOF-SIMS depth profiles (starting from the P3HT:PCBM surface) for the device that was illuminated in a dry $^{18}O_2$:N_2 atmosphere: C_3^- (PCBM, with a possible contribution from P3HT) and ZnO_2^- (ZnO). The profiles were normalized against the total intensity to remove possible instrument effects. The profiles labeled "$^{18}O_2$" and "$H_2{}^{18}O$" are the $^{18}O/^{16}O$ intensity ratio profiles for the devices that were exposed to a dry $^{18}O_2$:N_2 or an oxygen free $H_2{}^{18}O$:N_2 atmosphere. The vertical dashed line represents the P3HT:PCBM−ZnO interface.

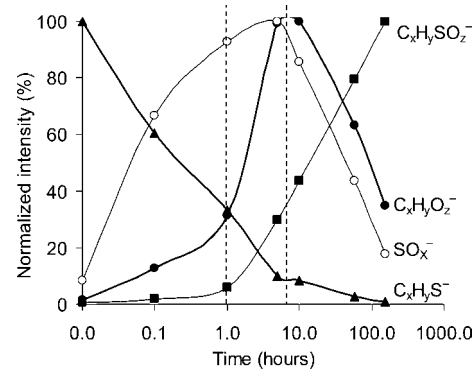

Figure 10. TOF-SIMS intensity plots for fragment ions obtained on a P3HT:PCBM surface for various exposure times (1000 W m^{-2}, 72 ± 2 °C) in ambient air (43 ± 5% rh). The "*x*", "*y*", and "*z*" indicate that a series of signals show the same behavor. Each point is an average of five measurements on different surface locations. The standard deviations are not shown for clarity.

A rule of thumb is useful in this situation: a lower signal-to-noise ratio suggests a higher ^{18}O uptake, so the two ZnO surfaces (i.e., P3HT:PCBM−ZnO interfaces indicated by a vertical dashed line in Figure 9) have most likely, to a higher degree, reacted with $^{18}O_2$ or $H_2{}^{18}O$ as compared to the bulk P3HT:PCBM material.

The closest one can possibly relate the $^{18}O/^{16}O$ profiles in Figure 9 to something absolute quantitative, are the corresponding values presented in Figure 7, which should correspond to 0 h sputter time in Figure 9. The semiquantitative difference between the $^{18}O/^{16}O$ profiles in Figure 9 is in agreement with the results presented in Figure 7. It was not possible to explain why an initial increase is observed in both $^{18}O/^{16}O$ profiles. The subsequent $^{18}O/^{16}O$ decrease could possibly be explained from the emerging ZnO and ITO signals. ITO is known to dissolve in adjacent organic layers over time. The presence of ZnO and/or ITO would lower the $^{18}O/^{16}O$ profile due to the high contents of ^{16}O in those materials. It is evident from Figures 8 and 9 that the depth resolution is rather poor for longer sputter times, which could hide possible effects that are associated with a narrow sputter time window.

Temporal Considerations in Regard to Degradation Mechanisms. Figure 4 shows the oxygen uptake at various illumination times in ambient air for spin-coated materials used in the device type described in this work. Equivalent plots can be constructed on the basis of TOF-SIMS fragment ion intensities. This is shown in Figure 10 for P3HT:PCBM spin-coated onto glass. These should not be mistaken for depth profiles. The corresponding plots for P3HT are equivalent due to the P3HT enrichment at the P3HT:PCBM−air interface. Chemical changes that take place as a result of illumination will be manifested in the fragment ion intensities. Fragment ions are formed in the ionization part of the analysis process. From Figure 5a, it is evident that sulfur reacts with water and/or molecular oxygen during illumination in ambient air, which will increase the $C_xH_ySO_z^-$ and SO_x^- intensities as observed in Figure 10. As a consequence, the $C_xH_yS^-$ ions originating from the intact P3HT are observed to decrease in intensity. The increase in $C_xH_yO_z^-$ intensities suggest that either the thiophene carbon becomes oxygenated (reacts with water and/or molecular oxygen) or (more probably) the side chains are oxygenated. It is very difficult, based on TOF-SIMS data alone, to conclude on the specific details of the mechanisms. The important observation is the fact that after ∼1 and ∼7 h some of the trends change. This could be interpreted as new degradation processes/mechanisms that are starting to appear and/or that old processes/mechanisms are disappearing. The most drastic change is observed for SO_x^- and $C_xH_yO_z^-$ that are observed to decrease after ∼7 h. One possible explanation could be that the population of R−SO_x moieties decreases as a result of gaseous SO_2 and SO_3 formation. Furthermore, at some point, one would intuitively expect the intact side-chain population to become exhausted, which could possibly explain the decrease in $C_xH_yO_z^-$ after ∼7 h. The plots in Figure 10 neatly demonstrate that not all degradation processes take place continuously to the same extent and, at the same time. A specific degradation process can be restricted to a time window, that is, a photon dose window. It is thus important to consider the illumination dose when studying degradation of materials. The observations described earlier in this work are good examples of this fact. Introduction of a barrier layer such as PEDOT:PSS will significantly impede water and/or molecular-induced degradation of P3HT:PCBM, which is manifested in the lack of some degradation reactions (Figure 6). According to the information extracted from Table 2 and Figures 5 and 6, it was concluded that during the lifetime of the devices that were studied in this work, it was not possible to detect formation of sulfoxides, and only ∼3% of the carbon was observed to transform to R−COOH (presumably mainly from the side chains). The processes that are described in Figure 10 are therefore most likely not representative of the degradation processes that take place during the lifetime of the devices during operation and would be expected after very extended periods of testing complete devices.

Oxygen Uptake − Effect of Storing Time. The two nonencapsulated devices that were illuminated in a dry $^{18}O_2$:N_2 or oxygen free $H_2{}^{18}O$:N_2 were monitored over time with respect to the $^{18}O/^{16}O$ ratio on three surfaces: (i) the PEDOT:PSS surface (between the silver stripes, Figure S5), (ii) the P3HT:PCBM surface (after removal of the PEDOT:PSS layer, Figure S5), and (iii) the ZnO surface (after removal of the P3HT:PCBM layer). The oxygen uptake in ZnO could not be quantified due to the saturated ^{16}O signal. As an alternative, the ratio was monitored by setting the zero time $^{18}O/^{16}O$ value to 100%. The ^{16}O saturation on the ZnO surface is assumed to be the same for all measurements. The result is presented in Table 3. Intuitively, one would expect to observe either an unchanged ratio or a decrease. ^{16}O can be added from ambient molecular

Table 3. TOF-SIMS Measured $^{18}O/^{16}O$ Ratios for the Two Devices That Were Illuminated (330 W m^{-2}, 72 ±2 °C) in $^{18}O_2$:N_2 or $H_2{}^{18}O$[a]

analyzed surface	atmosphere	0 months (%)	1.3 months (%)	6.3 months (%)
PEDOT:PSS	$^{18}O_2$:N_2	100 ± 5	94 ± 5	86 ± 14
PEDOT:PSS	$H_2{}^{18}O$:N_2	100 ± 2	135 ± 12	191 ± 119
P3HT:PCBM	$^{18}O_2$:N_2	100 ± 5	96 ± 3	20 ± 3
P3HT:PCBM	$H_2{}^{18}O$:N_2	100 ± 7	187 ± 18	87 ± 8
ZnO	$^{18}O_2$:N_2	100 ± 10		19 ± 1
ZnO	$H_2{}^{18}O$:N_2	100 ± 1		33 ± 2

[a] The PEDOT:PSS surface was analyzed between the silver stripes, the P3HT:PCBM surface was analyzed after removal of the PEDOT:PSS layer, and the ZnO surface was analyzed after removal of the P3HT:PCBM layer. Each surface was analyzed over 6.3 months, and the ratio is given in percent relative to the first measurement. Each value is an average of five measurements on different surface locations.

oxygen and/or water. Reacted ^{18}O could be removed if it came from a reversible process, or if it reacts further with ambient molecular oxygen and/or water forming volatile compounds (e.g., $CO^{18}O$). The only situation one would not expect is an increase in the $^{18}O/^{16}O$ ratio because ^{18}O cannot be specifically added from the ambient. However, this is exactly what is observed for the PEDOT:PSS surface illuminated in the $H_2{}^{18}O$ atmosphere.

One possible explanation could be that an oxygen-containing compound present in PEDOT:PSS that did not react with $H_2{}^{18}O$ was slowly removed from the analyzed surface. Excess PSS is known to segregate and is thus a candidate, assuming it did not react with $H_2{}^{18}O$. It could also be one or more of the additives in PEDOT:PSS. The corresponding increase in the standard deviation suggests that the ^{18}O reaction products become more heterogeneously distributed on the surface over time. The other PEDOT:PSS surface ($^{18}O_2$:N_2) exhibits the opposite behavior; that is, the $^{18}O/^{16}O$ ratio decreases over time.

In light of the strange behavior for the corresponding PEDOT:PSS surface from the $H_2{}^{18}O$ atmosphere, it is difficult to elaborate further, especially because PEDOT:PSS contains unknown additives. This led us to further study the PEDOT:PSS using two-dimensional imaging as shown in Figure 11. Figure 11 also shows the result of an experiment where two partial devices (ITO-ZnO-P3HT:PCBM-PEDOT:PSS) were illuminated without encapsulation for three weeks in a dry $^{18}O_2$:N_2 or an oxygen free $H_2{}^{18}O$:N_2 atmosphere (Figure 11a−d) or in a $H_2{}^{18}O$ atmosphere (Figure 11e−h). The TOF-SIMS images of the PEDOT:PSS surfaces reveal that the layers have phase separated into a PEDOT-rich and a PSS-rich phase. Each phase was identified from area-specific TOF-SIMS mass spectra (not shown). Figure 11b shows that $^{18}O_2$ reacted almost exclusively with PEDOT, and Figure 11c reveals that it is at least the sulfur in PEDOT that significantly reacted with $^{18}O_2$. Figure 11a shows the in-plane distribution of ^{16}O that originates primarily from the $-SO_3H$ group in PSS. According to the mass spectrum (not shown), the $-SO_3H$ group did not exchange oxygen with $^{18}O_2$. Figure 11e−h shows the corresponding images for the partial device that was exposed to a $H_2{}^{18}O$ atmosphere. The phase separation is not as clear, but still visible. $H_2{}^{18}O$ appears to react to a much lesser extent and not mainly with one phase. The oxygen incorporation can be semiquantitatively compared from the $^{18}O/^{16}O$ ratios. Because PEDOT and PSS contain different amount/types of ^{16}O (natural oxygen), the entire surfaces are compared. The $H_2{}^{18}O$ exposed surface has an $^{18}O/^{16}O$ ratio of 2% (as compared to the "natural" ratio of 0.2%), and the $^{18}O_2$ exposed surface has an $^{18}O/^{16}O$ ratio of 15%. Any difference observed (other than oxygen incorporation) in the mass spectral data between the two surfaces must be related to chemical changes induced/caused by the atmosphere. One such difference was observed (not shown). One of the unknown additives in PEDOT:PSS is a fluorinated carbon species (most possibly a detergent material), which according to the mass spectral data (not shown) seem to be surface enriched for the $H_2{}^{18}O$ exposed surface. The $F/^{16}O$ ratios demonstrate this very well. The $^{18}O_2$ exposed surface has an $F/^{16}O$ ratio of 8%, and the $H_2{}^{18}O$ exposed surface has an $F/^{16}O$ ratio of 157%. Because the identity of the fluorinated carbon species is unknown, it is difficult to give firm conclusions, but the gradual surface enrichment in the presence of water concurs with the idea, and we ascribe the surface enrichment to be due to migration of fluorinated nonionic detergents to the surface in humid atmospheres, whereas they do not diffuse in dry atmospheres (or to a much lesser extent). In summary, the phase separation is more pronounced when a dry $^{18}O_2$:N_2 atmosphere is used as compared to an oxygen free $H_2{}^{18}O$:N_2 atmosphere. Because phase separation is observed for both atmospheres, it is likely a heat-induced phenomenon possibly affected to some extent by the atmosphere. $H_2{}^{18}O$ is causing surface enrichment of an unknown fluorinated carbon species. $^{18}O_2$ reacts mainly with PEDOT, and at least with the sulfur functionality. $H_2{}^{18}O$ reacts nonspecifically and to a much lesser extent as compared to $^{18}O_2$. As a consequence of the phase separation, PEDOT becomes less shielded by PSS and thus more susceptible toward $^{18}O_2$-induced degradation. Furthermore, the in-plane degradation pattern in the sublayers is identical to the PEDOT pattern (not shown), which suggests that oxygen is mainly diffusing trough the PEDOT phase. This phenomenon could explain why the inverted devices (ITO-ZnO-P3HT:PCBM-PEDOT:PSS-Ag) have a short lifetime in an O_2:N_2 atmosphere, and a relatively long lifetime in a H_2O atmosphere; that is, the phase separation deteriorates the barrier properties with respect to O_2 and favors transport of oxygen through the PEDOT phase with faster and selective oxidation at that interface. Incidentally, the PEDOT phase is also the phase that conducts the electrical current, thus implying that transport is more quickly impeded. From an OPV stability point of view, this phase separation is clearly undesirable, and countermeasures should be implemented possibly via a modified version of PEDOT:PSS that is more resilient toward phase separation or alternatively an alternative to PEDOT:PSS.

Except for one discrepancy (Table 3, P3HT:PCBM, $H_2{}^{18}O$, 1.3 months), the $^{18}O/^{16}O$ ratios for the P3HT:PCBM surfaces are observed to decrease over time with little effect on the homogeneity. There is a significant difference in the $^{18}O/^{16}O$ ratios between the two P3HT:PCBM surfaces after 6.3 months, the surface from the dry $H_2{}^{18}O$:N_2 atmosphere exhibits only a small decrease (87% of the original value) and the surface from the $^{18}O_2$:N_2 atmosphere exhibits a significant decrease of 20%, which suggests that different ^{18}O reaction products were formed during illumination, which is intuitively consistent with the expectations.

The ZnO surfaces are simpler; they are expected (like other metal oxides) with ease[37] to exchange the incorporated ^{18}O with ^{16}O, which is consistent with the observations (Table 3). Intuitively, one would not expect the 6.3 months values to be the same, because the exchange mechanisms with $^{18}O_2$ and $H_2{}^{18}O$ are different. Exchange with $^{18}O_2$ is expected to take place through trapping of superoxide radicals at the surface of the ZnO nanoparticles, whereas exchange with $H_2{}^{18}O$ is expected

(37) Lira-Cantu, M.; Norrman, K.; Andreasen, J. W.; Krebs, F. C. *Chem. Mater.* **2006**, *18*, 5684–5690.

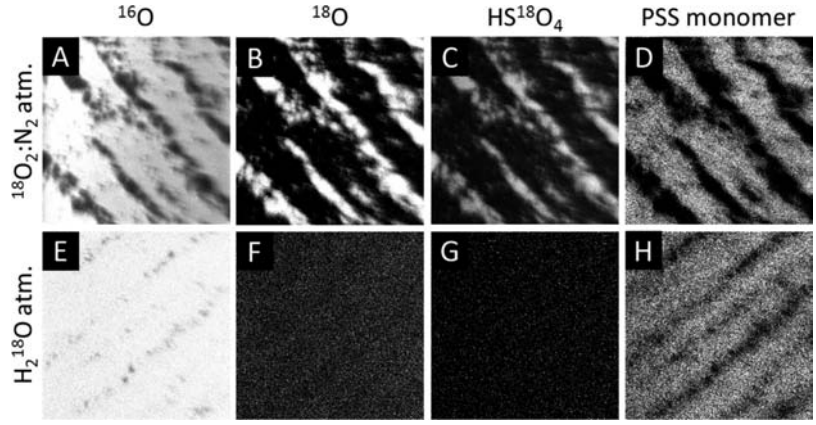

Figure 11. TOF-SIMS ion images (500 × 500 μm^2) of PEDOT:PSS surfaces from partial devices with the composition ITO-ZnO-P3HT:PCBM-PEDOT:PSS (no Ag electrode). The devices were illuminated (AM1.5, 330 W m^{-2}, 65 ± 2 °C) without encapsulation for 3 weeks in a dry $^{18}O_2$:N_2 (1 atm) atmosphere (A−D) or in an oxygen free $H_2{}^{18}O$:N_2 (65 ± 2% rh) atmosphere (E−H). Black corresponds to 0% signal, gray to some signal, and white to 100% signal.

to take place through exchange of hydroxide on the surface of the ZnO nanoparticles.

The findings in Table 3 demonstrate that time is an important factor after illumination in an isotopically labeled atmosphere; one should not store the samples for too long. To illustrate the importance, the two devices in question were stored in darkness in a vacuum for 90% of the 6.3 months and in ambient air in darkness for the remaining time, which was sufficient to affect the ^{18}O contents significantly for some of the surfaces/materials.

Conclusions

Water- and oxygen-induced degradation of an inverted polymer solar cell (ITO−ZnO−P3HT:PCBM−PEDOT:PSS−Ag) was studied using XPS and TOF-SIMS in conjunction with the isotopically labeled atmospheres $H_2{}^{18}O$ and $^{18}O_2$:N_2 that provided detailed information on where and to what extent degradation had occurred in the devices. For direct exposure to illumination in ambient air, it was found that P3HT, PCBM, P3HT:PCBM, and PEDOT:PSS all experience oxygen uptake over time, more specifically, the formation of R−SO_x and R−COOH species along with various other oxygenated carbon species. However, PEDOT:PSS both gains and looses oxygen; initially oxygen loss outweighs the oxygen gain that later becomes the dominant process. It was found that during the lifetime of the devices the extent of oxygen uptake is less than the uncertainty of the XPS measurement. TOF-SIMS data were thus calibrated against XPS data that enabled a low-level of oxygen to be measured. For both devices, it was found that during the lifetime of the devices no detectable R−SO_x species are formed in P3HT:PCBM and PEDOT:PSS, and only a few percent of the carbons had been oxygenated in P3HT:PCBM, which presumably constitute some of the side chains. The lowest oxygen uptake (0.001 atom %) during the lifetime was found for P3HT:PCBM for the device that was kept in darkness, and the highest oxygen uptake (0.3 atom %) was found for PEDOT:PSS for the device that was kept in darkness. For $^{18}O_2$:N_2, the oxygen uptake increases for both PEDOT:PCBM and PEDOT:PSS when illuminated as compared to storing under equivalent conditions but in darkness. For oxygen free $H_2{}^{18}O$:N_2, the behavior is opposite, as illumination decreases the oxygen uptake, which is ascribed to a temperature effect. TOF-SIMS depth profiling revealed that $H_2{}^{18}O$ and $^{18}O_2$ both had reacted throughout the P3HT:PCBM layer and had accumulated at the P3HT:PCBM−ZnO interface. The reactivity of $^{18}O_2$ toward P3HT:PCBM was approximately twice the $H_2{}^{18}O$ reactivity under the conditions in question. The complex nature of degradation processes was demonstrated by monitoring the temporal development of degradation for P3HT:PCBM. Not all degradation processes take place continuously to the same extent, and at the same time, a specific degradation process can be restricted to a time window, that is, a photon dose window. It was shown that during storing of the devices in darkness after all the measurements were done, the materials change over time. PEDOT:PSS was found to phase separate, and the PEDOT and the PSS phases showed different reactivity toward oxygen with selective oxidation of the PEDOT phase and subsequent oxidation throughout the device layers beneath the PEDOT phase. We thus demonstrated that for the inverted devices the major failure mechanism is related to the PEDOT:PSS phase separation and the PEDOT:PSS−active layer interface. We tentatively ascribe this to the necessary presence of surface active materials in the PEDOT:PSS formulation, which leads to dynamic electrical behavior as a function of the atmospheric conditions. The possible implications of this are that PEDOT:PSS should be sought replaced in the context of polymer solar cells or reformulated to remove the dynamic dependence of the performance on the relative humidity.

Acknowledgment. This work was supported by the Danish Strategic Research Council (DSF 2104-05-0052 and 2104-07-0022), EUDP (j. nr. 64009-0050), and PV-ERA-NET (project acronym POLYSTAR).

Supporting Information Available: Experimental details. Variation in V_{oc}, I_{sc}, and FF with step changes in humidity. Electric resistance and relative humidity versus time for a PEDOT:PSS film. Electric resistance versus relative humidity for a PEDOT:PSS film. TOF-SIMS ion image showing the in-plane distribution of ITO in the P3HT:PCBM layer close to the ZnO interface. This material is available free of charge via the Internet at http://pubs.acs.org.

JA106299G